A TWO-PART SEARCH FOR SLOW-MOVING OBJECTS[a]

JANE X. LUU[b,c] AND DAVID JEWITT[b]
Department of Earth, Atmospheric, and Planetary Sciences, Massachusetts Institute of Technology, Cambridge, Massachusetts 02139
Received 7 October 1987; revised 22 December 1987

ABSTRACT

We have carried out a preliminary, two-part survey of the outer solar system by searching for slow-moving objects (apparent opposition motion $\leqslant 10''$/hr) using two Schmidt telescopes and a 1.3 m telescope equipped with a charge-coupled-device (CCD) camera. Objects as faint as 24th magnitude were imaged with the CCD. The survey yields empirical 99% confidence limits to the projected surface density of objects in the outer solar system of $S < 1.7\times10^{-2}$ deg^{-2} for $m_V \leqslant 20$, and $S < 15$ deg^{-2} for $m_R \leqslant 24$. The survey and the derived limits are discussed.

I. INTRODUCTION

The gravitational sphere of influence of the Sun extends to $R \approx 2\times10^5$ Astronomical Units (AU) (Weissman 1986), but the effective boundary of the planetary system is much smaller, presently being defined by Pluto at $R \approx 40$ AU. The only objects postulated beyond Pluto are the Oort Cloud comets, with a mean semimajor axis $R \approx 2\times10^4$ AU (Marsden *et al.* 1978). Very little is known about the contents of the outer solar system. For example, besides the planets, only one object classified as an asteroid (2060 Chiron) is known to have a semimajor axis greater than that of Saturn ($R \approx 10$ AU). There is no compelling theoretical reason why the planetary system should end at the orbit of Pluto and, in any case, it is difficult to believe that the outer solar system is an empty void, as current observations suggest. Instead, it seems likely that the apparent emptiness is an observational artifact and that many bodies remain to be discovered in the vicinity of the giant planets and beyond.

Two systematic searches have been made specifically for astronomical bodies in the outer solar system. An early survey by Tombaugh covered a large fraction of the northern sky to photographic magnitude $m_{pg} \approx 18$ (Tombaugh 1961). The primary result of Tombaugh's work was, of course, the discovery of Pluto in 1930. No additional objects beyond the orbit of Saturn were reported. A more recent wide-field survey was made by Kowal (1979) using the Palomar 48 in. Schmidt; this survey yielded the most distant known asteroid, 2060 Chiron (although classified as an asteroid, the composition of Chiron remains unknown, and it could in fact be a large comet). No other objects beyond Saturn have been reported from this survey, and the details of Kowal's work remain unpublished, as far as we know. It is to be noted that the surveys by Tombaugh and Kowal were designed to look for slow-moving objects. There have been other photographic surveys (discussed below), but these have typically been directed towards the investigation of main-belt asteroids, and the observers involved were not specifically searching for more distant (slow-moving) objects. In 1983, the *Infrared Astronomical Satellite* (*IRAS*) was used to carry out a survey of the inner solar system, and the results of a search for *fast*-moving objects in the *IRAS* data have been published by Green *et al.* (1985). The results of a search for *slow*-moving *IRAS* objects have yet to be reported.

In recent years, to explain various dynamical puzzles (i.e., the unexplained perturbations in Neptune's orbit; the inefficient mechanism by which comets are transported from their presumed place of origin near Neptune to the Oort Cloud), astronomers have postulated the existence of undiscovered bodies in the outer solar system. Most notably, they have suggested the existence of an inner Oort Cloud in the Uranus–Neptune region (Whipple 1964; Safronov 1972; Fernandez 1980; Bailey 1983) or another trans-Neptunian planet (Planet X). Unfortunately, none of the recent hypotheses have been subjected to stringent observational testing, basically because little suitable observational material is available.

Motivated by the lack of a strong observational constraint on the contents of the outer solar system, we are conducting our own survey for slow-moving (distant) objects ("SMOs"). We define an SMO as any object having an apparent opposition motion $d\theta/dt \leqslant 10$ arcsec per hr, corresponding approximately to heliocentric distance $R \geqslant 10$ AU (beyond Saturn). Our two-part search uses the twin 0.6 m/0.9 m Schmidt telescopes at Kitt Peak and CTIO to study large areas of sky to moderate magnitudes ($m_V \approx 20$), and the McGraw–Hill 1.3 m telescope with a charge-coupled-device (CCD) detector to study a smaller area to fainter limits ($m_R \approx 24$). The Schmidt plates are about one hundred times less sensitive than the CCD images, but the area of sky imaged by each plate is about one thousand times the area covered by a CCD image, so that both plates and CCD data can provide useful constraints on the population of SMOs. The data from the two surveys are used to establish a limit on the number density for objects in the outer solar system.

II. OBSERVATIONS

The observed fields were selected to simultaneously satisfy three criteria:

(i) The fields were chosen to be in the ecliptic. This is the only plane near which solar system bodies are likely to be concentrated, if at all. (Arguments can be presented that favor the invariable plane of the solar system, or the plane of the orbit of Jupiter, over the plane of the ecliptic. However,

[a] Observations taken at the McGraw–Hill Observatory, Kitt Peak, which is operated by a three-university consortium consisting of University of Michigan, Dartmouth College, and MIT.

[b] Visiting Astronomer, Kitt Peak National Observatory, National Optical Astronomy Observatories, operated by the Association of Universities for Research in Astronomy, Inc., under contract with the National Science Foundation.

[c] Visiting Astronomer, Cerro Tololo Inter-American Observatory, National Optical Astronomy Observatories, operated by the Association of Universities for Research in Astronomy, Inc., under contract with the National Science Foundation.

0004-6256/88/041256-07$00.90

these planes are sufficiently close to the ecliptic that it seems reasonable to confine our initial search near the latter plane). If the outer solar system bodies are not confined to a special plane (like the comets in the spherically symmetric Oort Cloud), then the ecliptic is as good a place to look as any.

(ii) The fields were chosen to be near opposition. This criterion allows the distance to an object to be directly estimated from its apparent motion, mostly due to parallax. If it is assumed that the orbits of the Earth and SMO are concentric, coplanar circles, the apparent motion (radian/s) of the SMO at opposition is

$$\frac{d\theta}{dt} = \frac{v_{\rm Earth} - v_{\rm SMO}}{1.5\times 10^8 \Delta},$$

where $v_{\rm Earth}$ ($\approx$30 km/s) is the Keplerian velocity of the Earth, $v_{\rm SMO} = v_{\rm Earth}/R^{1/2}$ is the Keplerian velocity of the SMO, and R (AU) and Δ (AU) are its heliocentric and geocentric distances. At opposition, $\Delta = R - 1$ and so the apparent opposition motion, in arcsec/hr, is given by

$$\frac{d\theta}{dt} = 148\left(\frac{1 - R^{-0.5}}{R - 1}\right), \quad (1)$$

where $R > 1$. Additional advantages are that opposition fields are observable for the largest number of hours per night, and phase darkening is minimized.

(iii) The fields were chosen to be at high Galactic latitudes. This criterion was imposed to facilitate the identification of SMOs against the stellar background. The greater the number density of stars, the greater the problem of confusion and the more difficult it becomes to locate moving objects; for that reason, a search near the Galactic equator is practically impossible. At 60° Galactic latitude, the projected surface density of stars brighter than $m_{\rm pg} \approx 20$ diminishes by about a factor of 25 relative to the density at the Galactic equator (Allen 1981).

a) Schmidt Observations

The 0.6/0.9 m Schmidt telescopes at Kitt Peak National Observatory and Cerro Tololo Inter-American Observatory were both used in the direct camera mode. These telescopes are optical twins, so that photographic plates from the two are directly comparable. The image scale at the $f/3.5$ focal plane of each telescope is 96 arcsec/mm. The photographic plates were 194 mm $\times$ 194 mm square (corresponding to 5.2° $\times$ 5.2°). The fine-grain IIIa-F and IIIa-J emulsions were used, chosen for their sensitivity and low fog density. After hypersensitization by baking in a 2% hydrogen–nitrogen gas mixture, the plates were exposed unfiltered for typical times on the order of 60 min. The exposed plates were developed in D19 for 5 min following a systematic dark-room procedure.

The Schmidt plates were taken during dark time in February, March, and May 1987. Table I gives the field coordinates and dates of the observations. Generally, three plates were taken of each selected field, with a time difference between plates of at least 1 day. The 1 day timebase was used to detect relative motion, while the third plate was used for cross-checking purposes when needed. The Schmidts were manually guided at sidereal rate. We estimate that the Schmidt reached $m_V \approx 20$ on stationary (stellar) objects, and the image quality was consistently good over an entire plate. During 12 nights of observation with the Schmidts, we obtained 12 good fields that could be blinked; one field was subsequently rejected because of differences between the plates caused by atmospheric variations.

We examined the Schmidt plates using the Gaertner blink comparator at Kitt Peak National Observatory (KPNO), Tucson. The task of blinking the plates was time consuming and placed considerable strain on the eyes; on the average, each pair of plates required 8 hr of blinking. Most fields were blinked separately by both observers for thoroughness. Many factors complicated our search of the plates, including variations in the sky brightness from night to night, different fog densities on plates from different boxes, changes in the atmospheric seeing from night to night, spurious images from multiple internal reflections in the Schmidt optics, genuine emulsion defects, and, especially, dust specks on the emulsion.

On the average, we detected about 50–80 main-belt asteroids on each plate pair. Main-belt asteroids in low-eccentricity orbits located at $R = 2$–3 AU would exhibit an apparent motion $d\theta/dt \approx 30$–40 arcsec/hr (Eq. (1)). Therefore, typical main-belt asteroids at this distance range appear on a 60 min plate as 0.3–0.4 mm trails. When blinked together, two Schmidt plates taken 1 day apart reveal main-belt asteroids as two 0.3–0.4 mm trails separated by about 7–10 mm. Asteroids moving in inclined and eccentric orbits will exhibit angular motion somewhat different from the model numbers quoted above. Nevertheless, characteristic rapid motion clearly distinguishes the main-belt asteroids from the SMOs of the present study, which should appear as two $\leqslant$0.1 mm trails separated by $\leqslant$2.5 mm. A large number of objects that seemed to have substantially smaller than main-belt motion were marked and later examined under a microscope. Without exception, these slower-moving objects proved to be dust specks or emulsion defects.

b) CCD Observations

The 390 $\times$ 584 pixel MASCOT (MIT Astronomical Spectrometer Camera for Optical Telescopes) was mounted as a direct camera at the $f/7.5$ Cassegrain focus of the 1.3 m telescope at McGraw–Hill Observatory, Kitt Peak. The MASCOT CCD is characterized by low readout noise (12 electrons per pixel), negligible dark current, and good linearity of response. A particularly important feature of the MASCOT–1.3 m combination for our work was the unusually high throughput—approximately 20%, including reflection losses from the primary and secondary telescope mirrors, losses from the MASCOT internal optics, quantum efficiency of the CCD, and transmission through the atmosphere and through the Mould R filter used for all images.

The resulting image scale on the CCD chip was 2.26 arcsec/pixel. Because of vignetting inside the MASCOT, the area of the CCD chip used for observations was limited to 242 $\times$ 276 pixels; therefore, the useful field of view was 9.1′ $\times$ 10.4′ (95 sq. arcmin). The large image scale was chosen to obtain as large a field of view as possible, while avoiding dramatic undersampling of the point-spread function of the telescope and atmosphere. In practice, the full width at half-maximum of stellar images was comparable to or less than the pixel size, so that star images were formally undersampled by a factor of order 2 (as judged by the Nyquist criterion).

Using the 1.3 m telescope at McGraw–Hill Observatory, we took four consecutive exposures of an ecliptic field on a given night, then two more consecutive exposures of the same field the next night to detect very slow-moving objects. The telescope was autoguided at sidereal rate and photome-

TABLE I. Fields observed with Schmidt telescopes.

Field	R.A.	Dec	Emulsion	Plate no.	Date	Exposure
ECL 1	11h00	+05°00	IIIa-F	15917	21 / 02 / 87	43 min
				15919	22 / 02 / 87	60 min
				15922	22 / 02 / 87	45 min
				15925	23 / 02 / 87	60 min
ECL 2	09h30	+15°00	IIIa-F	15918	22 / 02 / 87	60 min
				15921	22 / 02 / 87	60 min
				15924	23 / 02 / 87	60 min
ECL 3	10h30	+10°00	IIIa -F	8639	22 / 03 / 87	35 min
				8640	23 / 03 / 87	55 min
				8643	24 / 03 / 87	55 min
ECL 4	12h00	00°00	IIIa-F	8641	23 / 03 / 87	55 min
				8644	24 / 03 / 87	55 min
ECL 5	12h30	-03°00	IIIa-F	8642	24 / 03 / 87	55 min
				8645	24 / 03 / 87	55 min
ECL 6	11h30	+03°00	IIIa-J	30949	27 / 05 / 87	55 min
				30953	28 / 05 / 87	60 min
				30956	30 / 05 / 87	60 min
ECL 7	13h00	-05°00	IIIa-J	30954	28 / 05 / 87	60 min
				30960	31 / 05 / 87	60 min
				30965	01 / 06 / 87	60 min
ECL 8	13h30	-10°00	IIIa-J	30961	31 / 05 / 87	60 min
				30966	01 / 06 / 87	40 min
				30967	02 / 06 / 87	60 min
ECL 9*	14h00	-13°00	IIIa-J	30951	27 / 05 / 87	60 min
				30955	28 / 05 / 87	45 min
				30957	30 / 05 / 87	60 min
				30968	02 / 06 / 87	60 min
ECL 10	15h00	-17°00	IIIa-J	30963	31 / 05 / 87	60 min
				30969	02 / 06 / 87	60 min
ECL 11	16h00	-21°00	IIIa-J	30952	27 / 05 / 87	60 min
				30958	30 / 05 / 87	60 min
				30962	31 / 05 / 87	60 min
				30970	02 / 06 / 87	60 min
ECL 12	12h09	-00°40	IIIa-F	30883	24 / 04 / 87	45 min
				30902	27 / 04 / 87	55 min

* rejected from survey

try was obtained from the images using nearby Landolt stars for calibration (Landolt 1983). No attempt was made to record flatfield exposures for the present data. This unusual decision was permissible because sensitivity differences among the pixels of the uniphase TI chip used for all observations are small ($<10\%$ across the full width of the chip, and generally $\leqslant 1\%$ on scales $\leqslant$tens of pixels) and, most importantly, because the blink analysis performed on the CCD images (see below) effectively negates all deviations from flatness. The neglect of flatfields provides an advantage in terms of improved signal-to-noise ratio in the images.

An integration time of 20 min was deemed optimum for our program; in this time, celestial objects brighter than $m_R = 24$ were consistently imaged in successive CCD images. A longer integration time would have allowed us to go deeper, but at the expense of fewer fields and under the penalty of a larger trailing loss. In 20 min, an SMO with apparent motion $d\theta/dt \leqslant 10''$/hr would trail with respect to field stars by $\leqslant 1.5$ pixels, slightly more than a seeing disk. The trailing loss on this or any slower object is negligible (a few $\times$ 0.1 mag). By comparison, the trailing loss in a 60 min image of an SMO could approach 1 mag. Main-belt asteroids, with apparent motion $d\theta/dt \approx 30''$–$40''$/hr, suffer comparably large trailing losses even in the 20 min integrations.

We obtained 70 images of 14 independent fields during five nights of observations in 1987 April. The coordinates and dates of the CCD images are listed in Table II. One field was discarded because seeing and transparency variations occurred during the image sequence and made comparison of the images impractical. A typical trail due to a main-belt asteroid is illustrated in Fig. 1 [Plate 72], which is the difference of two consecutive CCD frames. Difference pictures of the type shown in the figure were useful for identifying the brighter main-belt asteroids in the CCD data. However, we found that rapid sequential blinking of consecutive CCD frames was a much more effective method for finding faint moving targets.

We examined the CCD images at KPNO with the software package "IRAF", using a four-plane image display. On this display, we could blink four images in rapid succession (blink interval 0.5–1.0 s), facilitating the rejection of spurious candidates for SMOs. Any candidate that did not appear in all frames was ignored, as was any object that failed to exhibit uniform motion between each of the four successive images. Of order 200 cosmic-ray hits were detected in each CCD image. Fortunately, it proved easy to distinguish the cosmic rays from astronomical sources because cosmic-ray hits are sharp, often only one pixel in area, whereas all astronomical objects appear broadened by atmospheric turbulence. Furthermore, the probability that four random cosmic rays might hit four consecutive CCD frames in such a way that they simulate the motion of an asteroid is $\ll 10^{-6}$ (i.e., negligible). All CCD fields were blinked by both observers to ensure accuracy. No SMOs were found.

TABLE II. Fields observed with CCD.

Field	R.A.	Dec	Date	# Images
1	12:00:00.3	- 00°00'05"	21 / 04 / 87	5
2	13:30:11.2	- 08°56'35"	22 / 04 / 87	4
3	14:00:09.3	- 12°01'43"	22 / 04 / 87	4
4	16:00:12.8	- 20°02'24"	22 / 04 / 87	4
5	10:59:51.1	+06°01'00"	23 / 04 / 87	4
6	13:19:48.6	- 08°01'28"	23 / 04 / 87	4
			24 / 04 / 87	2
7	13:50:05.8	- 11°59'34"	23 / 04 / 87	4
			24 / 04 / 87	2
8	14:30:10.6	- 15°07'17"	23 / 04 / 87	4
			24 / 04 / 87	2
9	11:20:06.7	+04°04'19"	24 / 04 / 87	4
10	14:15:03.6	- 13°47'18"	24 / 04 / 87	4
			25 / 04 / 87	3
11	14:45:02.4	- 16°00'08"	24 / 04 / 87	4
			25 / 04 / 87	2
12	16:00:10.3	- 22°02'12"	24 / 04 / 87	1
			25 / 04 / 87	1
			27 / 04 / 87	4
13*	12:30:03.0	- 02°58'21"	25 / 04 / 87	4
			27 / 04 / 87	2
14	16:00:42.0	- 18°02'38"	27 / 04 / 87	3

* rejected from survey

III. RESULTS

We observed 11 Schmidt fields, of total area 297 sq. deg or 7.2×10^{-3} of the whole sky; with the 1.3 m, the observed area was 0.338 sq. deg or 8.2×10^{-6} of the sky. Numerous ($\approx$700) main-belt asteroids were found on the Schmidt plates but no SMOs were identified. The CCD fields yielded 11 main-belt asteroids, but again no SMOs were detected.

The heliocentric distances of the main-belt asteroids found with the CCD were estimated from their apparent motions using Eq. (1). The radii of the asteroids were calculated from the radius–magnitude relation

$$p\,a^2 = 2.25\times10^{16}\ R^2\Delta^2 10^{0.4(m_{\rm Sun}-m)}, \qquad (2)$$

where $p = 0.1$ is the adopted geometric albedo, $m_{\rm Sun}$ ($m_V = -26.74$, $m_R = -27.26$) is the magnitude of the Sun (Allen 1981), a (km) is the radius, R (AU) is the heliocentric distance, Δ (AU) is the geocentric distance, and m is the apparent magnitude. Table III lists the objects found, their magnitudes, derived heliocentric distances, and approximate radii. The slowest (furthest) asteroid was of magnitude $m_R \approx 22.0$–22.5 and had an apparent motion $d\theta/$

TABLE III. Faint main-belt asteroids from the CCD data.

Object no.	Magnitude m_R	Apparent motion [arcsec / hr]	Heliocentric Distance [AU]	Radius* [m]
1	21.0 - 21.5	30 ± 2	3.2 ± 0.3	600 - 740
2	21.0 - 21.5	50 ± 2	1.7 ± 0.1	100 - 130
3	21.0 - 21.5	43 ± 2	2.0 ± 0.1	170 - 210
4	20.6	38 ± 2	2.4 ± 0.2	430 ± 100
5	18.8	37 ± 2	2.4 ± 0.2	980 ± 230
6	21.0 - 21.5	41 ± 2	2.2 ± 0.1	220 - 280
7	22.0 - 22.5	30 ± 2	3.2 ± 0.3	370 - 470
8	19.6	54 ± 2	1.5 ± 0.1	150 ± 40
9	18.6	38 ± 2	2.3 ± 0.1	950 ± 120
10	20.6	41 ± 2	2.2 ± 0.1	340 ± 45
11	22.0 - 22.5	29 ± 2	3.3 ± 0.3	400 - 510

*radius computed using p = 0.1

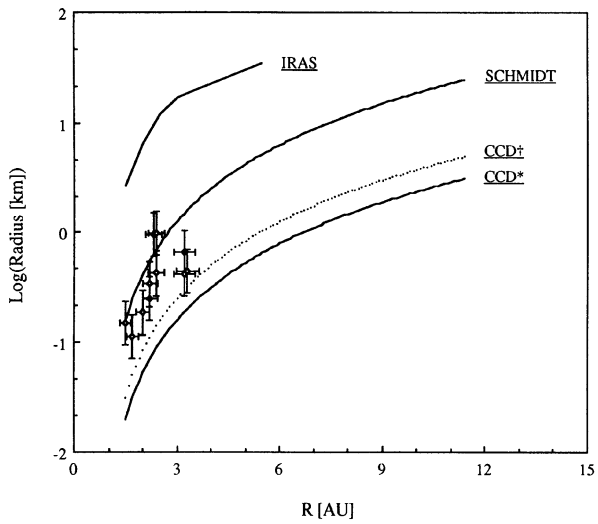

FIG. 2. Radius versus heliocentric distance for faint asteroids detected in the CCD survey. The solid lines (*IRAS*, Schmidt, CCD*) represent the detection limits of *IRAS* (Green *et al.* 1985) and our program for stationary objects; the dashed line (CCD†) represents the CCD detection limit for main-belt asteroids and includes a correction for the trailing loss. The geometric albedo is assumed to be $p = 0.1$.

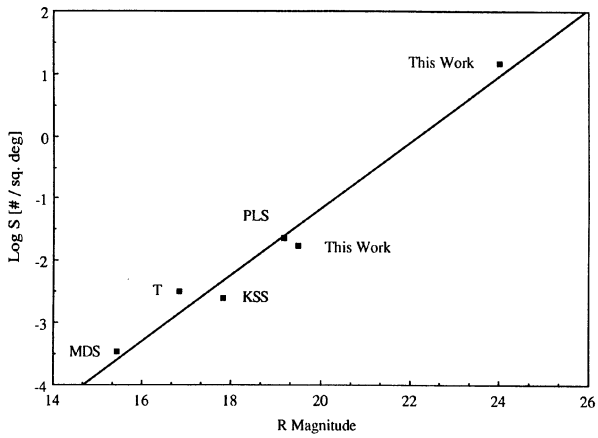

FIG. 3. Empirical 99% confidence limits to the cumulative surface density of slow-moving objects ($d\theta/dt \leqslant 10$ arcsec/hr) plotted as a function of apparent magnitude. Symbols in the graph have the following meanings: MDS = McDonald Survey, PLS = Palomar–Leiden Survey, KSS = Kiso Schmidt Survey, T = Tombaugh. The solid line is a least-squares fit to the data, added solely to guide the eye.

$dt \approx 29''$ per hour, corresponding to $R = 3.3 \pm 0.3$ AU. The asteroids were found to be very small, the majority having radius $a < 1$ km. Within the uncertainties of measurement, the number of small main-belt asteroids found with the CCD is comparable to the number expected based on an extrapolation of the magnitude distribution of the Palomar–Leiden Survey (van Houten *et al.* 1970).

The radii of the main-belt asteroids are plotted against their heliocentric distances in Fig. 2, together with the curves representing the detection limits of the *IRAS* survey (Green *et al.* 1985) and of the present Schmidt and CCD surveys. Solid lines in the figure were calculated for stationary or slow-moving objects, for which the trailing loss is negligible. The single dotted line indicates the approximate detection limit for the CCD when used to observe main-belt asteroids trailing at $d\theta/dt = 30''$/hr, and includes an appropriate trailing-loss correction. It may be seen that, as expected, the detected asteroids cluster close to this effective detection limit, rather than at the limit for stationary objects.

No SMOs were found in 297 sq. deg of sky examined to magnitude 20 in the present Schmidt survey, and none were detected in 0.338 sq. deg (1217 sq. arcmin) of sky examined to magnitude 24 in the CCD survey. Since no SMOs were found, we can place only statistical upper limits to the cumulative surface densities from the Schmidt data and the CCD data. Assuming a Poisson distribution for the number of SMOs per unit area, we can state within a 99% certainty (roughly corresponding to a 3σ upper limit) that our results imply the following surface-density limits:

$$S_{m=20} < 1.7 \times 10^{-2} \text{ deg}^{-2}, \quad (3)$$

$$S_{m=24} < 15 \text{ deg}^{-2}. \quad (4)$$

IV. DISCUSSION

The empirical cumulative surface-density limits given in Eqs. (3) and (4) are plotted in Fig. 3, together with 99% confidence limits obtained from other sources. The other sources are the McDonald Survey (no SMOs found in 14 400 sq. deg; Kuiper *et al.* 1958), the Palomar–Leiden Survey (no objects in 216 sq. deg; van Houten *et al.* 1970), the Kiso Schmidt Survey (no objects in 1944 sq. deg; Ishida *et al.* 1984) and the asteroid search in the ecliptic by Tombaugh (1961; no objects in 1530 sq. deg). Although only the searches by Tombaugh and Kowal were explicitly directed towards the detection of SMOs, we include the other published surveys under the (perhaps naïve) assumption that these observers would have noticed SMOs had they been present. The survey by Kowal is omitted from Fig. 3 in the absence of a formal published account of his work. Figure 3 summarizes the current empirical constraints on the surface density of objects in the outer solar system down to about red magnitude 24. The limits in Fig. 3 are reasonably well fit by a power law (straight line); no physical significance should be attached to this fit, however.

It is interesting to consider what limits the data in Fig. 3 might place on the population of bodies in the outer solar system. Clearly, the R^{-4} dependence of the scattered light (see Eq. (5)) will not allow this survey to place meaningful constraints on objects in the outer Oort Cloud (a Halley-like nucleus at $R \approx 10^4$ AU would have apparent magnitude $m_R \approx 54$), but objects at smaller distances, in the vicinity of the orbit of Neptune, for instance, or in a "comet belt" (Whipple 1964) might be detected. To address this question in a simple but specific way, we assume a Sun-centered, spherically symmetric model for the SMOs, similar to the Oort Cloud, with a number density independent of radius. Using this simple model we calculate upper limits for N_m, the total number of objects brighter than some magnitude m_0, as well as n[#/AU^3], the number density, and $\mathcal{M}$ [Earth masses/AU^3], the mass density.

An object with radius a, geometric albedo p, at heliocentric distance R and geocentric distace Δ will have a magnitude m given by the radius–magnitude relation (Eq. (2)). At opposition, $\Delta = R - R_E$, where R_E is the distance between the Earth and the Sun. For distant objects ($R \gg R_E$) we may write:

$$m_0 \approx m_{\rm Sun} - 2.5 \log \frac{p\,a^2}{2.25\times 10^{16}\,R^4}. \quad (5)$$

All objects of radius a at heliocentric distance smaller than R will have magnitude $m < m_0$. Assuming a uniform spherical distribution and that the size distribution of objects adopts the form of a power law, $n(a)da = C\,a^{-\alpha}\,da$, we can write an expression for dN_m, the number of objects with radius in the range a to $a + da$ having heliocentric distance $\leqslant R$:

$$dN_m = n(a)\frac{4}{3}\pi R^3\,da = C\,a^{-\alpha}\frac{4}{3}\pi R^3 da. \quad (6)$$

Since, by definition, we are only interested in the region $R \geqslant 10$ AU (beyond the orbit of Saturn), we rewrite dN_m for a spherical shell, substituting for R in terms of m_0 from Eq. (5):

$$dN_m = C\,a^{-\alpha}\frac{4}{3}\pi(R^3 - R_{\rm Sat}^3)da = \frac{4}{3}\pi C\,a^{-\alpha} \times\left\{\left[\frac{p\,a^2}{10^{0.4(m_{\rm Sun}-m_0)}2.25\times 10^{16}}\right]^{3/4} - R_{\rm Sat}^3\right\}da, \quad (7)$$

where $R_{\rm Sat} = 10$ AU is the inner radius of the shell. Integrating over all possible a gives N_m, the total number of objects with magnitude $m \leqslant m_0$

$$N_m = \int dN_m = \frac{4}{3}\pi C\left\{\left[\frac{p}{10^{0.4(m_{\rm Sun}-m_0)}2.25\times 10^{16}}\right]^{3/4} \times\int_{a_{\rm min}}^{\infty} a^{-\alpha+3/2}da - R_{\rm Sat}^3\int_{a_{\rm min}}^{\infty} a^{-\alpha}\,da\right\}. \quad (8)$$

Here, $a_{\rm min}$ is the radius of an object located at $R = R_{\rm Sat} = 10$ AU, having an apparent magnitude $m = m_0$, where $m_0 = 20$ for the Schmidt data and $m_0 = 24$ for the CCD data. With $p = 0.1$, the calculated minimum radii are $a_{\rm min} = 19$ km for $m_0 = 20$ and $a_{\rm min} = 2.4$ km for $m_0 = 24$.

The limiting surface densities (Eqs. (3) and (4)) imply that 99% confidence upper limits to the total number of objects beyond Saturn brighter than the magnitude limits of the Schmidt and the CCD are $N(m_0 = 20) < 680$ and $N(m_0 = 24) < 6.1\times 10^5$, respectively. Substituting these values on the left-hand side of Eq. (8) gives a value for the constant C in the power law $n(a)\,da = C\,a^{-\alpha}\,da$. The size distribution index, α, is a free parameter of the model. Calculations were performed for several α in the range $2.6 \leqslant \alpha \leqslant 4.0$. None of these α is physically preferred, but we note with interest that the asteroid size distribution is approximately matched by an $\alpha = 2.8$ power law (Hartmann 1969).

The results of the calculations are summarized in Table IV. For each index α and limiting magnitude m_0, we present the limiting value of the constant C (from Eq. (8)), and the limiting number density of objects n[#/AU^3] obtained by integrating the size-distribution power law over all sizes $a > a_{\rm min}$. The final column lists the limiting detectable mass per unit volume $\mathcal{M}$[$\mathcal{M}_{\rm E}$/AU^3] (the mass of the Earth is $\mathcal{M}_{\rm E} = 6.0\times 10^{24}$ kg) obtained from

$$\mathcal{M} = \frac{4}{3}\pi\rho\,C\int_{a_{\rm min}}^{a_{\rm max}} a^{3-\alpha}da, \quad (9)$$

where density $\rho = 10^3$ kg m^{-3} is assumed. Here, $a_{\rm max}$ is taken arbitrarily to be 100 km, the size of a very large comet nucleus, in order to apply our measured densities to the hypothesis of an inner Oort Cloud.

Within the narrow context of the present spherical, uniform cloud model, a few conclusions may be drawn from Table IV. First, the limits on the number density obtained from the Schmidt data are about 10^3 times stronger than the limits obtained from the CCD data. This is a result of the smaller field of view of the CCD compared to the field of the Schmidt. Second, the limiting mass densities are about 10^{-8}–10^{-9} $\mathcal{M}_{\rm E}$/AU^3 for the power law size distributions considered here. The density of the planetary system obtained by smearing the masses of the planets over a sphere of

TABLE IV. Derived 3σ limits to the SMO population.

Power Law index α	Limiting mag m_0	Power law constant C	Number density [# / AU^3]	Mass density [M_E / AU^3]
2.6	20	$< 4.3 \times 10^{-29}$ m$^{-1.4}$	< 0.013	$< 6.6 \times 10^{-10}$
	24	$< 1.4 \times 10^{-27}$ m$^{-1.4}$	< 11	$< 2.3 \times 10^{-8}$
2.8	20	$< 1.1 \times 10^{-27}$ m$^{-1.2}$	< 0.039	$< 1.8 \times 10^{-9}$
	24	$< 2.2 \times 10^{-26}$ m$^{-1.2}$	< 35	$< 4.3 \times 10^{-8}$
3.0	20	$< 1.5 \times 10^{-26}$ m^{-1}	< 0.067	$< 2.8 \times 10^{-9}$
	24	$< 2.0 \times 10^{-25}$ m^{-1}	< 59	$< 4.6 \times 10^{-8}$
3.5	20	$< 5.4 \times 10^{-24}$ m$^{-1/2}$	< 0.143	$< 4.5 \times 10^{-9}$
	24	$< 2.6 \times 10^{-23}$ m$^{-1/2}$	< 126	$< 3.3 \times 10^{-8}$
4.0	20	$< 1.4 \times 10^{-21}$	< 0.230	$< 5.6 \times 10^{-9}$
	24	$< 2.5 \times 10^{-21}$	< 202	$< 2.2 \times 10^{-8}$

radius 10 AU is $\rho_{ss} \approx 10^{-1}\ \mathscr{M}_E/\mathrm{AU}^3$. The limiting mass density is a function of the unknown a_{max}, but for any plausible choice of a_{max}, we find that the empirical densities are orders of magnitude less than ρ_{ss}. Third, the densities are comparable to or greater than the mean density of the Oort Cloud. If 10^{12} comets (Weissman 1986) of 10 km radius and density $\rho = 10^3$ kg m^{-3} are distributed over a sphere of radius 2×10^4 AU, the mean density is of order $10^{-11}\ \mathscr{M}_E/\mathrm{AU}^3$. Therefore, we conclude that the empirical limits set by existing surveys are sufficiently weak that they do not contradict the hypothesis that the Oort Cloud extends into the planetary region.

V. CONCLUSIONS

(1) No slow-moving objects ("SMOs") were detected in 297 sq. deg of sky examined to magnitude 20 using Schmidt plates. No SMOs were detected in 0.338 sq. deg (1217 sq. arcmin) of sky examined to magnitude 24 using a CCD on a 1.3 m telescope. Assuming a Poissonian surface-density distribution, these nondetections can be used to compute 99% confidence limits to the projected surface densities of SMOs. The limits are $S < 1.7 \times 10^{-2}$ deg^{-2} for $m_V \leqslant 20$ and $S < 15$ deg^{-2} for $m_R \leqslant 24$.

(2) Several faint main-belt asteroids with radii in the range 0.1–1 km were observed. The surface density of these asteroids was comparable to that obtained from an extrapolation of the Palomar–Leiden Survey to fainter magnitudes.

(3) Objects of red magnitude $m_R = 24$ can be detected in a 20 min integration using a standard CCD camera mounted on the McGraw–Hill 1.3 m telescope. At heliocentric distance $R = 10$ AU, this magnitude corresponds to an object having an albedo times cross-section product $p\pi a^2 \sim 1.8$ km^2. With $p = 0.1$, the radius of the smallest detectable object is $a = 2.4$ km. This is already substantially smaller than the size of the commonly studied main-belt asteroids, demonstrating the power of the CCD on a very modest telescope. Planned future efforts with CCDs on larger telescopes should improve the detection limit by at least a magnitude.

We thank the Kitt Peak and Cerro Tololo staffs for efficient assistance during our observing runs. We are grateful to George R. Ricker, Jr., for the use of the MASCOT CCD camera and to the McGraw–Hill staff for help with the equipment setup. This work was supported in part by a grant from the NSF.

REFERENCES

Allen, C. W. (1981). *Astrophysical Quantities*, 3rd ed. (Athlone, London), p. 243.
Bailey, M. E. (1983). Mon. Not. R. Astron. Soc. **204**, 603.
Fernandez, J. A. (1980). Mon. Not. R. Astron. Soc. **192**, 481.
Green, S. F., Davies, J. K., Eaton, N., Stewart, B. C., and Meadows, A. J. (1985). Icarus **64**, 517.
Hartmann, W. K. (1969). Icarus **10**, 201.
Ishida, K., Mikami, T., and Kosai, H. (1984). Publ. Astron. Soc. Jpn. **36**, 357.
Kowal, C. T. (1979). In *Asteroids*, edited by T. Gehrels (University of Arizona, Tucson), pp. 436–439.
Kuiper, G. P., Fujita, Y., Gehrels, T., Groeneveld, I., Kent, J., van Biesbroeck, G., and van Houten, C. J. (1958). Astrophys. J. Suppl. **3**, 289.
Landolt, A. U. (1983). Astron. J. **88**, 439.
Marsden, B. G., Sekanina, Z., and Everhart, E. (1978). Astron. J. **83**, 64.
Safronov, V. S. (1972). In *The Motion, Evolution of Orbits, and Origin of Comets*, edited by C.A. Chebotarev and E. I. Kazimirchak-Polonskaya (Reidel, Dordrecht), pp. 329–334.
Tombaugh, C. W. (1961). In *Planets and Satellites*, edited by G. P. Kuiper and B. M. Middlehurst (University of Chicago, Chicago), pp. 12–30.
van Houten, C. J., van Houten-Groeneveld, I., Herget, P., and Gehrels, T. (1970) Astron. Astrophys. Suppl. **2**, 339.
Weissman, P. R. (1986). In *The Galaxy and the Solar System*, edited by R. Smoluchowski, J. Bahcall, and M. S. Matthews (University of Arizona, Tucson), pp. 204–237.
Whipple, F. L. (1964). Proc. Natl. Acad. Sci. **51**, 711.

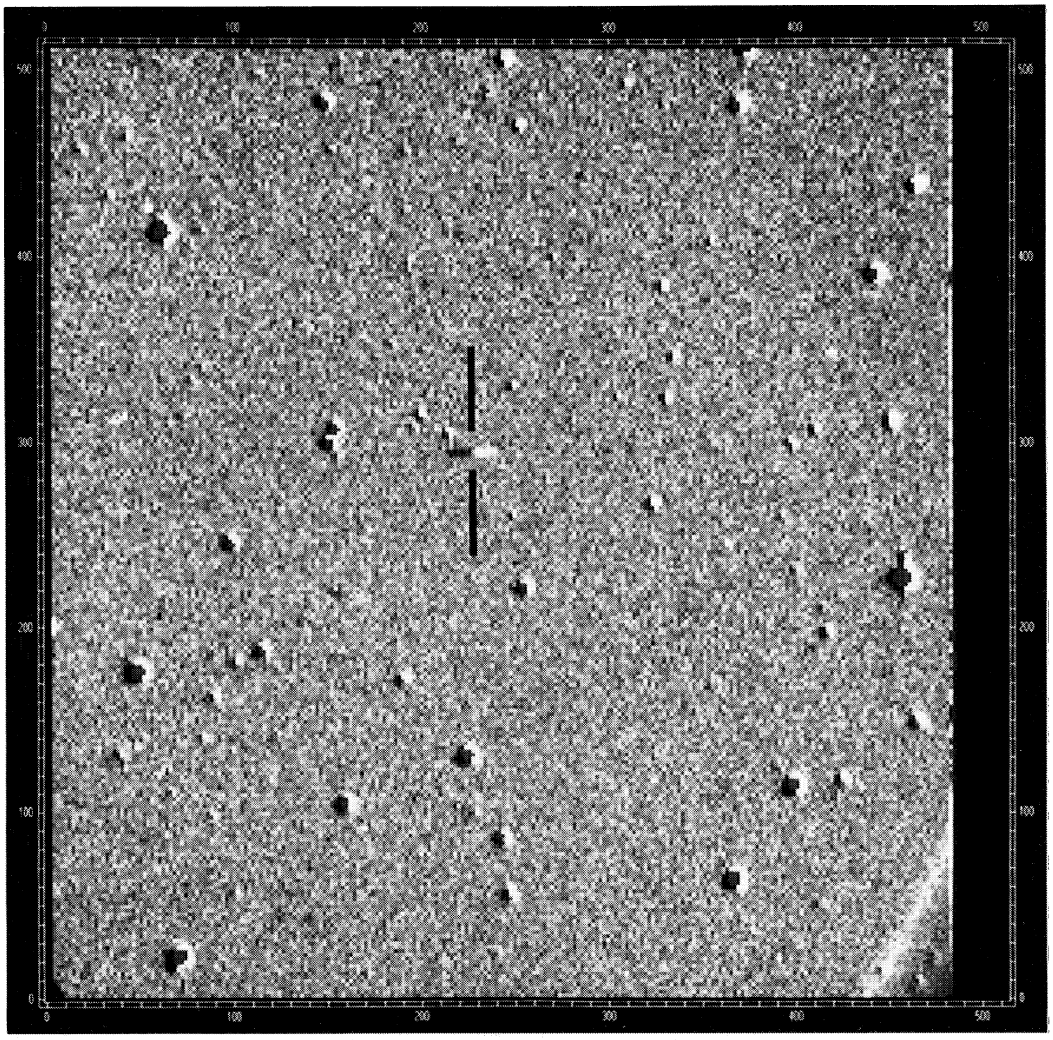

FIG. 1. Typical main-belt asteroid as seen by subtracting consecutive 20 min CCD integrations. The asteroid has $m_R \approx 19.6$, apparent motion $d\theta/dt \approx 54 \pm 2$ arcsec/hr, heliocentric distance $R \approx 1.5$ AU, and is estimated to have radius $a \approx 0.15$ km. North is toward the top of the figure, east toward the left, and the width of the field is 550″.

J. X. Luu and D. Jewitt (see page 1259)